

# Magnetocaloric Studies of the Peak Effect in Nb

N. D. Daniilidis,\* I. K. Dimitrov, V. F. Mitrović, C. Elbaum, and X. S. Ling<sup>†</sup>

*Department of Physics, Brown University, Providence, Rhode Island 02912*

(Dated: January 18, 2019)

## Abstract

We report a magnetocaloric study of the peak effect and Bragg glass transition in a Nb single crystal. The thermomagnetic effects due to vortex flow into and out of the sample are measured. The magnetocaloric signature of the peak effect anomaly is identified. It is found that the peak effect disappears in magnetocaloric measurements at fields significantly higher than those reported in previous ac-susceptometry measurements. Investigation of the superconducting to normal transition reveals that the disappearance of the bulk peak effect is related to inhomogeneity broadening of the superconducting transition. The emerging picture also explains the concurrent disappearance of the peak effect and surface superconductivity, which was reported previously in the sample under investigation. Based on our findings we discuss the possibilities of multicriticality associated with the disappearance of the peak effect.

PACS numbers: 74.25.Op, 74.25.Qt, 61.12.Ex

---

\*Corresponding author: nikos@brown.edu

<sup>†</sup>Corresponding author: xsling@brown.edu

## I. INTRODUCTION

One very fascinating result in condensed matter physics in recent decades is the understanding that, in spite of early predictions,[1] the long-range topological order associated with broken continuous symmetries can survive in systems with random pinning.[2, 3] In bulk type-II superconductors with weak point-like disorder the existence of a novel Bragg glass phase has been predicted.[3] This reaffirmed experimental facts known since the 1970s, that vortex lattices in weak-pinning, bulk, type-II superconductors can produce pronounced Bragg peaks in neutron diffraction.[4] Recent experiments[5, 6] have shown that a genuine order-disorder transition occurs in vortex matter. This transition appears to be the underlying mechanism of the well-known anomaly of the peak effect[7] in the critical current near  $H_{c2}$ . However there are still many outstanding issues concerning the Bragg glass phase boundary and the nature of the disordered vortex state above the peak effect.

Previous studies in a Niobium single crystal have revealed an intriguing picture of the peak effect in weakly-pinned conventional superconductors. Neutron scattering has shown that a vortex lattice order-disorder transition occurs in the peak effect region. This transition shows hysteresis and is believed to be first order, separating a low temperature ordered phase from a high temperature disordered one.[5] The hysteresis was not observed across the lower field part of the superconducting-to-normal phase boundary. Magnetic ac-susceptometry showed that at lower fields the peak effect disappears as well, indicating further connection between the peak effect and the order-disorder transition.[8] In addition, the line of surface superconductivity,  $H_{c3}$ , terminates in the vicinity of the region where the peak effect disappears. This picture is summarized in Fig. 1.

It was thus proposed that the peak effect is the manifestation of a first-order transition which terminates at a multicritical point (MCP) where the peak effect line meets a continuous, Abrikosov transition,  $H_{c2}$ . The MCP would be bicritical if a third line of continuous transitions ends there. The transition lines considered as a possible third candidate were a continuous vortex glass transition,  $T_{c2}$ , and the line of surface superconductivity. Alternatively, the MCP would be tricritical if the disordered phase is a pinned liquid with no high field transition into the normal state.[8] Subsequently, the disappearance of the peak effect at low fields has also been reported in other systems.[9, 10]

Thermodynamic considerations[8] suggest that the MCP is likely a bicritical point. Since

bicriticality implies the existence of competing types of order in the vortex system the question of which of the two lines,  $T_{c2}$  or  $H_{c3}$ , is relevant to the bicritical point has major importance. Its answer will provide insight into the disordered vortex state above the peak effect and the disordering transition itself. Evidently, the possible relevance of surface superconductivity to the destruction of bulk Bragg glass ordering, and hence the existence of the multicritical point, cannot be dismissed *a priori*. In fact it is well known that surface premelting plays an important role in solid-liquid transitions.[11]

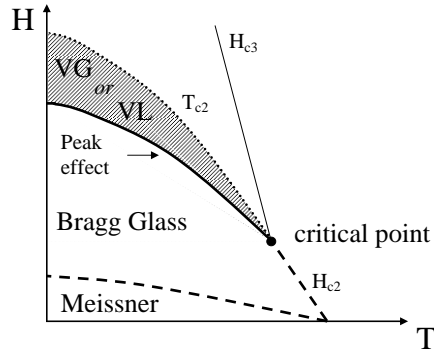


FIG. 1: A sketch of the phase diagram of the Nb single crystal from Park *et al.*[8]. Note the definitions of distinct  $T_{c2}$ ,  $H_{c2}$  and peak effect lines.

This issue could be resolved by repeating the ac magnetic susceptibility measurements after having suppressed surface superconductivity with appropriate surface treatment. Efforts to nondestructively achieve this, e.g. by electroplating the sample surface with a ferromagnetic layer, proved unfruitful, possibly due to high oxygen content of the surface. To address the problem, we performed measurements of magnetocaloric effects on the Nb single crystal studied by Ling *et al.*[5] and Park *et al.*[8]

Here we report a study of the peak effect using a magnetocaloric technique. Clear features associated with the peak effect, have been identified in the magnetocaloric data. We find that the superconducting to normal transition shows inhomogeneity broadening at all fields. The peak effect in the bulk critical current is found to disappear when it enters into the inhomogeneity broadened transition region. It is concluded that the concurrent disappearance of surface superconductivity and the peak effect is likely due to interference of surface superconductivity with the ac-susceptibility measurements. Nevertheless, the location of the MCP, as determined from magnetocaloric measurements, is in close vicinity to the location previously reported.[8] The transition across  $T_{c2}$  seems to be the same as that at

$H_{c2}$ , and surface superconductivity plays only a coincidental role in the critical point. This result suggests that the disordered vortex state, which is represented by the shaded part in Fig. 1, is a distinct thermodynamic phase. Bicriticality implies that this phase has an order parameter competing with that of the Bragg glass phase. We also discuss an alternative scenario, in which no critical point exists at any finite field or temperature.

The paper is organized as follows: In Sec. II we review the basic principle of magnetocaloric measurements, and give the experimental details of the sample and the technique used. In Sec. III we present our main results, discuss the consequences of irreversible and nonequilibrium effects on magnetocaloric measurements, and proceed to interpretation of the data and estimates of sample properties. Finally we summarize our findings and conclusions, and propose experimental work necessary to address the issues raised.

## II. EXPERIMENTAL

### A. Basic principle of magnetocaloric measurements

#### 1. *Heat flow in magnetocaloric measurements*

In studies of vortex phases in bulk superconductors, various experimental techniques provide complementary pieces of information. Combining these in a consistent picture is a non-trivial task. Magnetic ac-susceptibility measurements are sensitive to screening currents, and thus to the location of peak effect features, but are not suitable for the identification and study of the mean field  $H_{c2}$  transition itself.[8] Commercial magnetometers are not suited for study of large samples. Calorimetric[12, 13] and ultrasonic attenuation[14, 15] measurements determine the upper critical field where bulk condensation of Cooper pairs occurs, but it remains unclear under what circumstances they also provide a peak effect signature. Moreover the combination of information obtained with different techniques has to rely on thermometer calibration issues. Furthermore, the dynamical measurements suffer from thermal gradients in the studied samples. Magnetocaloric measurements overcome these difficulties because they are sensitive to both the presence of bulk superconductivity and to dynamical, flux-flow related effects. Moreover they can be performed in quasi-adiabatic conditions, where virtually no thermal gradients are present in the sample. Finally, they can be easily performed using a common calorimeter.

The magnetocaloric effect is a special case of thermomagnetic effects in the mixed-state of superconductors which have long been known and investigated.[16] These arise from the coexistence of the superconducting condensate which is not involved in entropy-exchange processes for the superconductor, and the quasiparticles, localized in the vortex cores, which are entropy carriers. Due to the presence of localized quasiparticles in the vortex cores, vortex motion results in entropy transport, which causes measurable thermal effects. Specifically, during field increase, new vortices are created at the edge of the sample, quasiparticles inside the vortices absorb entropy from the atomic lattice and cause quasi-adiabatic cooling of the sample. Conversely, during field decrease, the exiting vortices release their entropy to the atomic lattice, causing quasi-adiabatic heating.

Typically, in an experiment, the amount of entropy carried by the vortices entering or leaving the sample is not the exact thermodynamic equilibrium vortex entropy. The reason is that the vortex assembly is not equilibrated due to pinning as well as metastability associated with the underlying first-order phase transition at the peak effect. In practice, the magnetocaloric cooling and heating due to vortex entry and exit can be understood formally in terms of the actual entropy exchange between the vortex and atomic lattices. A superconductor subject to a changing magnetic field and allowed to exchange heat with the environment, undergoes a temperature change.[17] This process is described by the relation:

$$dQ_{abs}/dt = n T_s (\partial s / \partial H)_T dH/dt + n C_s dT_s/dt \quad (1)$$

where  $dQ_{abs}/dt$  is the net rate of heat absorption, positive for absorption of heat by the sample,  $n$  is the molar number of the superconductor,  $T_s$  its temperature,  $T_s (\partial s / \partial H)_T$  the molar magnetocaloric coefficient, and  $C_s$  the specific heat of the superconductor. The magnetocaloric term in the equation induces temperature changes. These are smeared out by the last term, describing the effect of specific heat. Nevertheless, in practice this last term is constrained to be negligible when magnetocaloric effects are measured. In our measurements, we use very low field ramp rates ( $dH/dt$ ), which result in very low temperature change rates ( $dT_s/dt$ ) causing the last term to be negligible.

A schematic of our setup is represented in Fig. 2a. In this setup, absorption or release of heat from the sample results in minute, but measurable, variation of its temperature. In a typical measurement, the sample temperature is first fixed at a selected value,  $T_{s0}$ . Subsequently, the field is ramped at a steady rate, resulting in quasi-adiabatic absorption

or release of heat from the sample. The resulting sample temperature change is recorded. If we neglect irreversible and non-equilibrium effects, the temperature change of the sample ( $\Delta T$ ) around its static value,  $T_{s0}$ , allows us to determine the molar magnetocaloric coefficient  $T_s(\partial s/\partial H)_T$  by use of:

$$-G_{\text{link}} \Delta T = n T_s (\partial s/\partial H)_T dH/dt \quad (2)$$

where the sample temperature  $T_s = T_{s0} + \Delta T$ , differential thermal conductance of the heat link  $G_{\text{link}}$ , molar number for the sample  $n$ , and field ramp rate  $dH/dt$  are all independently measured. The latter is positive for increasing fields, negative for decreasing fields.

## 2. Irreversible and non-equilibrium effects

In deriving the above equations we assumed that heat is only exchanged between the superconductor and the environment and that the superconductor reaches its quasi-static state as the measurement is performed. In an actual experiment, non-equilibrium and irreversible effects need to be considered. The heat generated by the dissipative processes between the vortex lattice and atomic lattice leads to a modification of the left hand side of equations 1 & 2. Non-equilibrium effects lead to a modification of the right hand side. While the effects of the Bean-Livingston surface barrier,[18] flux flow heating,[19] and the Bean critical state[20] can be complex and subtle, a detailed analysis can be performed and it will be discussed in Sec. III B 1. We show that the magnetocaloric measurements allow us to shed light into the problem of the peak effect in Nb that would not have been possible with any other single technique. In concluding this section, we note that since Eq. 2 is approximate, in what follows we refrain from using  $(\partial s/\partial H)_T$  to symbolize the quantity related to the magnetocaloric temperature change,  $\Delta T$ . Instead, we choose  $(ds/dH)$  to symbolize the measured “entropy” derivative.

## B. Sample and setup

We used a Nb single crystal sample with mass of 24.78 g which was previously studied using SANS and ac-susceptometry.[5, 8] It has an imperfect cylindrical shape (radius 0.5 cm, length 2.47 cm) with the cylinder axis oriented parallel to the [111] crystallographic direction. It has a  $T_c$  of 9.16 K and upper critical field  $H_{c2}(0) \approx 5600$  Oe, as previously reported.[5, 8]

We performed a zero field specific heat measurement, shown in Fig. 2b. This was done with the heat-pulse (relaxation) technique. From this measurement we obtain the Ginzburg-Landau parameter  $\kappa(0) = 3.8$  which is higher than the previous estimate[8]. In addition we find a superconducting transition width of 83 mK. The residual resistivity ratio from 300 K to 10 K of this sample is measured to be 12, suggesting a significant amount of defects in this Nb crystal. This is consistent with the large  $\kappa$  and upper critical field values.

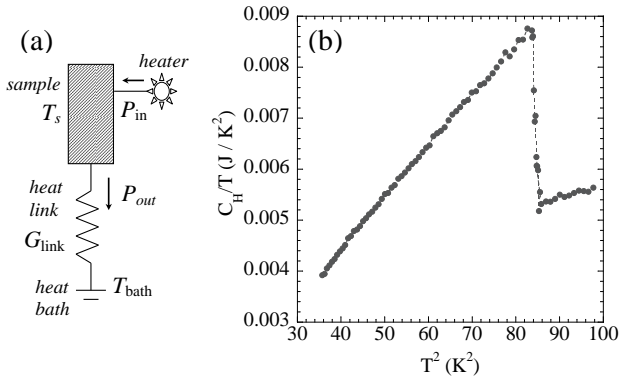


FIG. 2: (a) Idealized heat-flow diagram of the calorimeter used. (b) Specific heat of Nb crystal studied in zero applied field. The small contribution from the addenda of the calorimeter is included.

Our experimental setup is a homemade calorimeter and its idealized heat-flow diagram is shown in Fig. 2a. It consists of an oxygen-free, high-purity copper can which serves the role of a heat bath surrounding the sample. A piece of high-purity copper wire is used as a heat link between the sample and heat bath and the mechanical support for the sample is provided by nylon rods. During measurements, the heat bath is maintained at a temperature of 4.20 K and a carbon glass thermometer (Lakeshore) monitors its temperature. A second thermometer (Cernox, Lakeshore) is directly attached with silver epoxy to the lower end of the sample for reading the sample temperature. To minimize electronic noise in reading the thermometer resistance, high-frequency sinusoidal excitation together with pulse-sensitive detection is used. A Manganin wire, which is non-inductively wound on the sample and secured with Stycast epoxy, serves as a heater. A 50-turn high-purity copper coil is directly wound on the sample for simultaneous ac magnetic susceptibility measurement. During measurements the vacuum in the calorimeter is maintained to lower than 1 micron Hg by use of activated charcoal in thermal contact with the helium bath.

Calorimetric measurements are performed with the standard heat-pulse technique. The

heat input to the sample is increased incrementally, with step duration of 60-100 sec. Every incremental increase of the heat input results in exponential temporal relaxation of the sample temperature to its new equilibrium value. The sample heat capacity is determined through the decay time of the exponential. This technique offers moderate resolution and is not suited for studying the thermodynamics of the peak effect. Nevertheless, it allows us to characterize our sample. In Fig. 2b, we show the data acquired in zero applied field, from which we measured the sample properties quoted above.

During magnetocaloric measurements, a constant heat input,  $P_{in}$ , is supplied to the sample through the manganin heater, fixing the temperature at a selected static value,  $T_{s0}$ . After the sample temperature has stabilized to  $T_{s0}$ , the magnetic field is ramped up, then down, at a constant rate. During a field ramp, the sample temperature as a function of field,  $T_s(H)$ , is recorded. The magnetocaloric signal,  $\Delta T(H)$ , has to be measured with respect to a *field dependent*, static sample temperature reading:  $T_{s0} = T_{s0}(H)$ . This is the thermometer reading obtained at a given field,  $H$ , in the absence of field ramping. In other words one has to determine  $\Delta T(H) = T_s(H) - T_{s0}(H)$ . An example of raw data,  $\Delta T$  *vs.*  $H$ , is shown in Fig.3.

The field dependence of the  $T_{s0}(H)$  thermometer reading is a result of the following two effects: First, the magnetoresistance of the thermometer used. Second, a changing temperature gradient across the sample, as its field dependent thermal conductivity changes. This gradient can become considerable in the Meissner state for the highest measured temperatures ( $\approx 8$  mK / cm at 8.33 K). Nevertheless, it is negligible (less than 0.5 mK / cm) in the peak effect region which is the main focus of this paper. We stress here that the thermal gradient is a result of the external heat input  $P_{in}$ , not the magnetocaloric effect.

A possible variation of the heat input with applied field, which could be due to magnetoresistance in the heater, was investigated. It was verified that the heat input from the manganin heater does not vary by more than 1 part in  $10^4$  for the entire field range covered in any of our measurements.

The differential thermal conductance of the heat link between the sample and heat bath,  $G_{\text{link}}$  to be used in Eq. 2 above, is also measured at all temperatures of interest, for the entire range of applied fields. This is done through application of a small, pulsed heat input ( $P_{in} \pm \delta P_{in}$ ) to the sample and recording of the resulting temperature change, at different applied fields. The link conductance is found to vary smoothly by no more than 1 part in

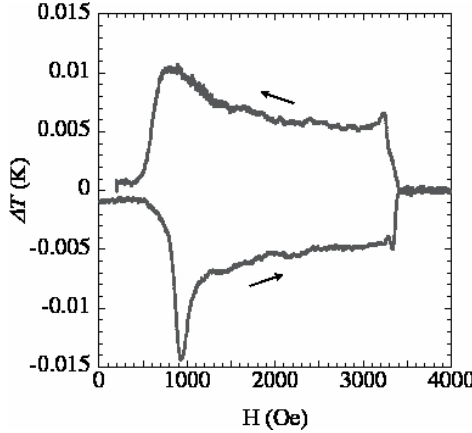


FIG. 3: Magnetocaloric temperature variation around  $T_{s0} = 5.37\text{K}$  *vs.* applied field, for increasing and decreasing field. The field ramp direction is indicated by arrows.  $dH/dt = 0.92\text{ Oe/sec}$  was used.

100 for the entire field range studied. This variation is insignificant compared to the random noise in the raw  $\Delta T$  data, and shall not be considered further.

Finally, the field ramp rate is measured through a resistor connected in series with the magnet coil, which allows us to monitor the current through the magnet. For all of the measurements presented here the ramp rate is 0.92 Oe/sec, which is the lowest possible with our system. At higher ramp rates, for example 1.87 Oe/sec, giant flux jumps occur in the sample.

### III. RESULTS AND DISCUSSION

#### A. Magnetocaloric results

##### 1. Main features in field scans

In Fig. 4a & b, we summarize the molar entropy derivative,  $(ds/dH)$ , measurements on increasing (a) and decreasing (b) fields, at different temperatures.  $(ds/dH)$  is calculated from the  $T_S(H)$  data following the procedure outlined above.

As indicated for the lowest temperature curve, 4.83 K (the upper most curve in Fig. 4a) several important features deserve attention. On increasing fields a peak occurs at low field. This is marked by  $H_1$ . It corresponds to the lowest field for vortex entry through a surface barrier. Its locus on the  $H - T$  plane closely follows the thermodynamic field, but occurs

slightly lower. This behavior is expected for a sample with finite demagnetizing factor and mesoscopic surface irregularities.[21] No corresponding peak is present on decreasing fields. Rather, a smoother increase of  $(ds/dH)$  occurs as the field is lowered, before entry of part of the sample into the Meissner state where the magnetocaloric signal vanishes, as seen in figures 3 & 4b.

In intermediate fields, we identify a novel feature which was not observed in previous magnetic susceptibility studies.[8] This appears as a knee in  $(ds/dH)$ , which shows larger negative slope as a function of field for fields lower than  $H_{\text{knee}}$ , as illustrated in Fig. 4c. The feature is the same for both field-ramp directions. With our setup we can identify the  $H_{\text{knee}}$  feature up to 7.41 K. As the temperature is increased, the region between  $H_1$  and  $H_{c2}$  narrows and it becomes increasingly difficult to discern  $H_{\text{knee}}$ . Thus it is unclear how this new feature terminates, i.e. whether it ends on the  $H_{c2}$  line at around  $H = 1000$  Oe, or if it continues to lower fields.

At high field, across  $H_{c2}$ , the equilibrium mean-field theory of Abrikosov predicts a step function for  $(\partial m/\partial T)_H$ .[26] Thus, in the simplest picture one would expect a simple step function for the molar entropy derivative  $(\partial s/\partial H)_T$  at  $H_{c2}$ . Instead, we observe that across the peak-effect regime, complex features of valley and peak appear in  $(ds/dH)$  below the field marked  $H_{c2}^{\text{up}}$ . The valley in  $(ds/dH)$  corresponds to the peak effect, as seen in Fig. 4. Similar features appear in decreasing field. At fields above the peak effect, the disappearance of the magnetocaloric effect marks the upper critical field,  $H_{c2}$ . As we will soon discuss, our magnetocaloric measurements indicate that the upper critical field shows inhomogeneity broadening, in agreement with the zero field calorimetric data mentioned in section II C. In Fig. 4 we mark with  $H_{c2}^{\text{up}}$  the upper end of the upper critical field. This is the value of field at which the magnetocaloric signal in the mixed state exceeds noise levels. Our technique is not sensitive to  $H_{c3}$  effects and the data are featureless above  $H_{c2}^{\text{up}}$ .

## 2. Identification of the peak effect

To verify the identification of the peak effect in our measurements, we performed simultaneous magnetocaloric and ac-susceptibility measurements, as shown in Fig. 5a. In the quasi-adiabatic magnetocaloric setup, the ac-amplitude used in this procedure has to be small. For large amplitudes inductive heating occurs in the mixed state on increasing  $dc$

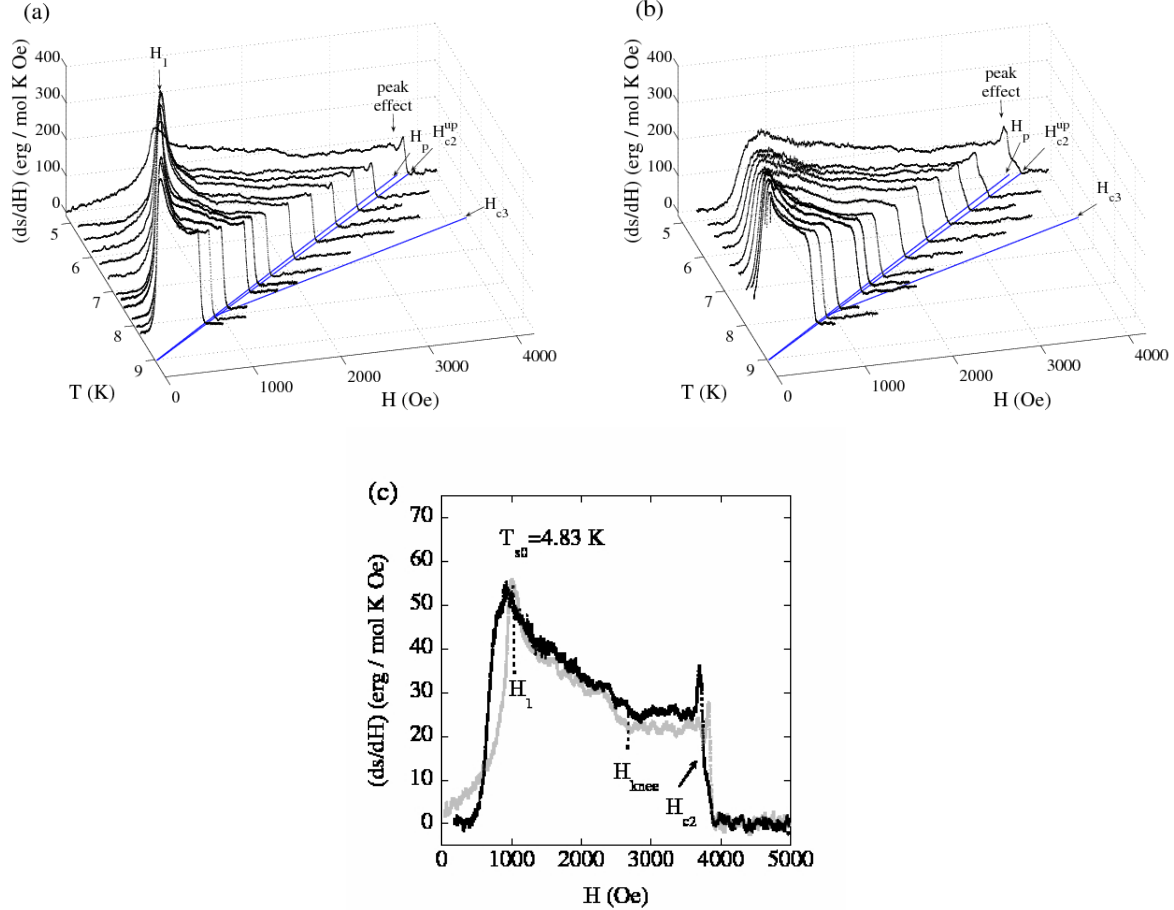


FIG. 4: (color online) Results of magnetocaloric measurements on (a) increasing and (b) decreasing field. Also shown (in blue) are the loci traced on the  $H - T$  plane by  $H_p$ ,  $H_{c2}^{\text{up}}$ , and  $H_{c3}$ . The  $H_{c3}$  line is drawn according to Park *et al.*[8]. (c) Full field scan at  $T_{s0} = 4.83$  K. Grey: Increasing field. Black: Decreasing field. The fields  $H_1$  and  $H_{\text{knee}}$ , and the region of the upper critical field, where the peak effect occurs, are marked.

field. Consequently the sample temperature increases rapidly by several degrees as the peak effect is crossed. This behavior is not surprising, but reaffirms that caution has to be taken when dynamic perturbations are combined with quasi-adiabatic measurements. We used an amplitude of 0.5 Oe at 107 Hz as a compromise between feasibility of the magnetocaloric measurement and resolution in the  $\chi'$  results. The results are shown in Fig. 5a.

In this combined measurement we find that both the onset and the peak of the peak effect have corresponding features. Moreover, we find no clear change in  $\chi'$  when the upper critical field, determined from the magnetocaloric measurement, is crossed. A slight change occurs

in the slope of the  $\chi'(H)$  curve across  $H_{c2}$ , but significant amount of screening, caused by surface superconductivity, remains when the bulk of the sample is in the normal state. This is a typical example of the inadequacy of ac-susceptometry in determining the upper critical field. Even with the use of larger ac fields the change in slope of  $\chi'(H)$  turns into a shoulder which does not reveal the exact location or characteristics of the bulk superconducting transition.[8].

### 3. Features of the peak effect

In light of the first-order transition underlying the peak effect, it is tempting to interpret the peak appearing in  $(ds/dH)$  at the peak effect as a manifestation of the entropy discontinuity of the transition. Nevertheless, a simpler interpretation exists in the context of critical state screening.

In specific, the magnetocaloric signature of the peak effect is consistent with critical-state[20] induced, non-equilibrium magnetization during the field ramps. The magnetocaloric valley-and-peak features in the peak-effect regime allow us to determine the positions of the onset,  $H_{\text{on}}$ , the peak,  $H_p$ , and the end,  $H_{\text{end}}$ , of the peak effect. We start with increasing field data. At low temperatures below 6.79 K where the peak effect is observed, the magnetocaloric signal starts dropping at the onset,  $H_{\text{on}}$ , of the peak effect. A minimum occurs in the vicinity of the peak of the peak effect,  $H_p$ , and it is followed by a peak, see Fig. 5b. This indicates slowing down, then acceleration of vortex entry into the sample, as the critical state profile becomes steep, then levels, in the peak effect region. Finally the magnetocaloric signal gradually drops to zero in the region of the upper critical field.

On decreasing field a magnetically reversible region exists for fields between  $H_{\text{end}}$  (the “end” of the peak effect) and  $H_{c2}^{\text{up}}$ . This is shown in Fig. 5b. Such behavior can be understood keeping in mind that the upper critical field in our sample is characterized by inhomogeneity broadening. We believe that the sliver of magnetic reversibility corresponds to the appearance of superconducting islands in our sample. These give rise to magnetocaloric effects, but they are isolated within the bulk and cannot support a screening supercurrent around the circumference of the sample, hence the reversible behavior. The “end” of the peak effect marks the onset of irreversibility and corresponds to a shoulder in the decreasing field curve. In the critical state screening picture, this occurs when continuous superconducting paths

form around the sample and a macroscopic critical current is supported. As the field is lowered below  $H_{\text{end}}$ , flux exit is delayed due to the increase in critical current, until past the peak of the peak effect, when accelerated flux exit results in a peak in  $(ds/dH)$  below  $H_p$ .

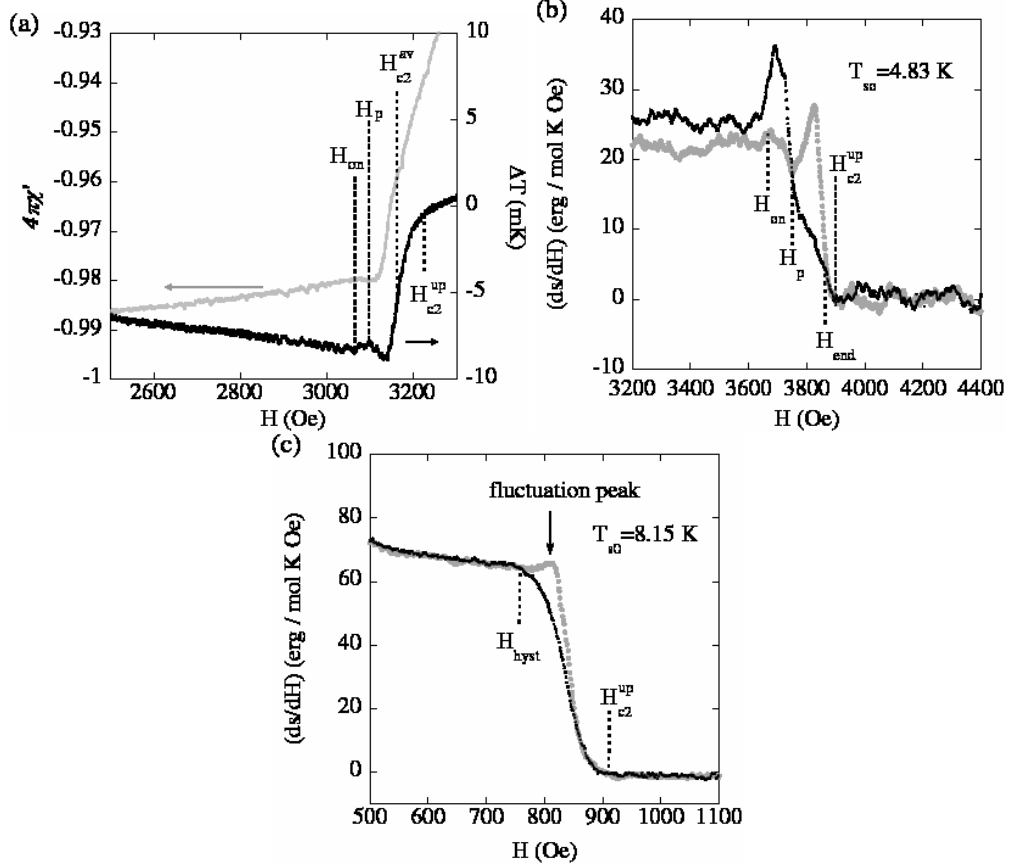


FIG. 5: (a) Magnetocaloric temperature variations and ac magnetic susceptibility as a function of increasing field, at  $T = 5.76$  K. The peak effect in  $\chi'$  is not pronounced due to the small ac amplitude used ( $h_{ac} = 0.5$  Oe,  $f = 107$  Hz). (b) Detail of magnetocaloric measurement in the upper critical field region at  $T = 4.83$  K. Grey: increasing field. Black: Decreasing field. (c) Same as b, at  $T = 8.15$  K.

#### 4. Fluctuation peak in $(ds/dH)$

In both field-ramp directions, the features due to the peak effect become less pronounced for higher temperatures, and finally disappear even before the previously identified[8] critical point is reached. On increasing fields, for  $T > 7.18$  K, a new peak appears in  $(ds/dH)$  just below the critical field, shown in Fig. 5c. This peak feature has already been reported in calorimetric measurements in pure Nb and  $\text{Nb}_3\text{Sn}$ .[12, 27] It has been attributed to

critical fluctuations in the superconducting order parameter which set in as the critical field is approached.[28] In our measurements we see the effect of critical-fluctuation entropy enhancement in  $(\partial s/\partial H)_T$ . We expect the same peak to exist in the curves displaying the peak effect feature, but its presence will be obscured by the dramatic results of non-equilibrium magnetization discussed above. Interestingly a similar peak is *not* observed on the decreasing field data, Fig. 5c. Moreover, it is evident in Fig. 5c, that apart from hysteretic behavior over an approximately 100 Oe wide region between  $H_{\text{hyst}}$  and  $H_{c2}^{\text{up}}$  the behavior of the sample is reversible to within noise levels. This behavior occurs consistently at all temperatures where the peak effect is not observed.

### 5. The superconducting to normal transition region

A very striking feature of our data is the invariance of the shape of the transition into (or out of) the bulk normal state with changing temperature, or critical field. For increasing fields, the transition into the normal state occurs between the fields  $H_0$  and  $H_{c2}^{\text{up}}$ , where  $(ds/dH)$  drops to zero monotonically, as shown in Fig. 6a. To illustrate this, in Fig. 6 we show the *normalized* entropy derivatives as a function of field for temperatures ranging from 4.83 K to 8.33 K, with an expanded view of the upper critical field region. The normalization has been performed such that the average of  $(ds/dH)_{\text{norm}}$  over a 50 Oe wide region below the onset of the peak effect equals unity. The curves have also been horizontally offset, on a  $\Delta H = H - H_{c2}^{\text{up}}$  axis. The horizontal alignment can alternatively be performed by aligning the ordinate of either  $H_0$ , or the part of the curve where the signal equals a given value, for example 0.1 in the normalized Y axis. All different criteria result in alignments differing by only a few Oe. The case is similar for decreasing fields.

In Fig. 6a we present increasing field data that display the peak effect on the normalized/offset axes. For comparison, one curve which does not display the peak effect has been included. This corresponds to T=7.41 K. In Fig. 6b we present the corresponding decreasing field data. In Fig. 6c we show only curves without a peak effect, for both increasing and decreasing field. These figures illustrate the uniform characteristics of the transition between the mixed state and the normal state. This is most evident in Fig. 6c: All different curves collapse onto one uniform curve for each field ramp direction. In figures 6a & b, the occurrence of the peak effect results in variations of the magnetocaloric signal around this

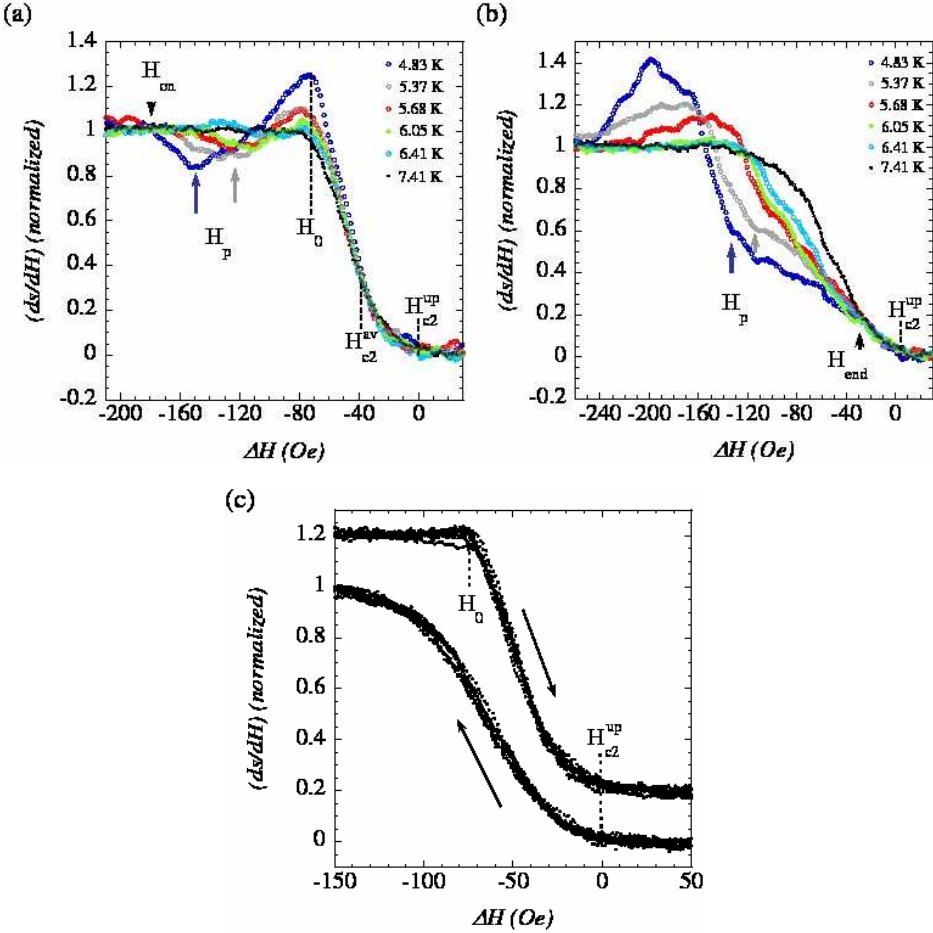


FIG. 6: (color online) Normalized entropy derivative  $(ds/dH)$  versus  $\Delta H = H - H_{c2}^{\text{up}}$ , for the magnetocaloric data in the upper critical field region.  $(ds/dH)$  is rescaled to unity in the  $\Delta H$  region between -300 and -250 Oe. (a) Increasing field data with and without the peak effect. The 7.41 K data do not show peak effect. (b) Same as a for decreasing field. (c) Collapsed magnetocaloric curves without peak effect, for increasing (top, vertically offset by +0.2) and decreasing (bottom) fields. Temperatures included: 7.18 K, 7.41 K, 7.55 K, 7.94 K, 8.15 K, 8.33 K.

uniform transition. These variations are, as already discussed, consistent with critical state induced flux screening on the field ramps. The uniformity of the transition for all field values implies that critical fluctuation broadening of the transition plays a minor role in our sample. Rather, inhomogeneity broadening seems to be the cause for the observed behavior.

As already stated in Sec. II, calorimetric measurements indicate inhomogeneity broadening to a width of approximately 83 mK for the zero field transition in our sample. With this in mind, we conclude that for increasing fields the gradual disappearance of the mag-

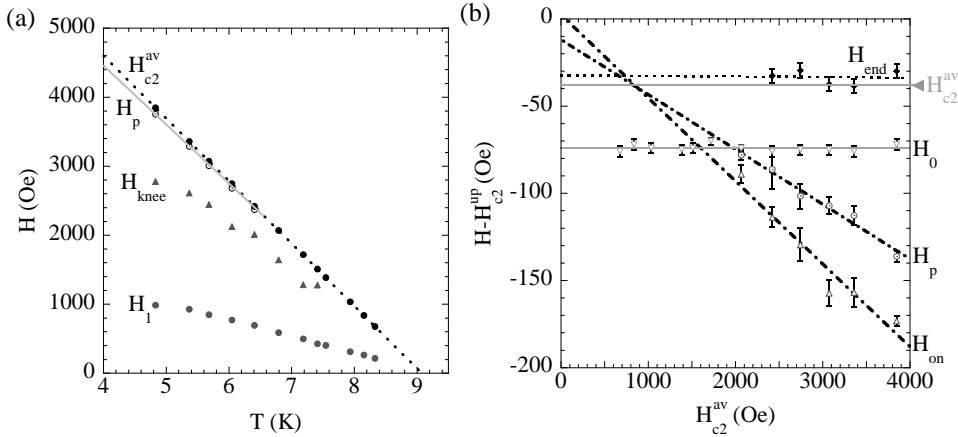


FIG. 7: Phase diagram obtained from magnetocaloric measurements. (a) The identified features in  $H - T$  axes, and linear fits through the  $H_p$  and  $H_c2^av$  lines. (b) Detail of the peak effect region: distance of peak effect features from the conventionally defined  $H_c2^up$  line, vs.  $H_c2^av$ .

netocaloric signal in the region between  $H_0$  and  $H_c2^up$  corresponds to the gradual loss of bulk superconductivity in our sample. In all of our measurements, the width  $H_c2^up - H_0$  is essentially constant around a mean of  $74.1 \pm 1.9$  Oe (Fig. 6a & c), which translates to a width of  $78.8 \pm 2.0$  mK on the temperature axis. This value is in good agreement with that obtained in the calorimetric measurement, given the finite temperature step of 10 to 15 mK used in the latter. Based on the identification of the lower and upper limits of the upper critical field, we identify the location of the mean field transition,  $H_c2^av$ , to be in the midpoint of the  $H_0$  to  $H_c2^up$  range, see Fig. 6a. Local variations in electronic properties in the sample cause broadening around this value. With this in mind we proceed to the discussion of the evolution of the peak effect.

#### 6. Disappearance of the peak effect in $(ds/dH)$

We already mentioned that in the magnetocaloric measurements the peak effect is not observed for temperatures above 7.18 K, or critical fields  $H_c2^av$  below 1718 Oe. The disappearance of the bulk peak effect at such high field seems to contradict the previous observation, from ac-susceptometry, that the peak effect occurs for fields as low as approximately 900 Oe.[8] Our current findings offer a resolution of this controversy.

To do this we trace the evolution of the positions of the onset and the peak of the peak effect versus  $H_c2^av$  in our increasing field data. We focus on increasing fields, because in these

the range of the upper critical field transition between  $H_0$  and  $H_{c2}^{\text{up}}$  is clearly discernible. The location of each of these features is identified by the intersection of two linear fits on different sections of the  $(ds/dH)$  curve. Each fit is performed in a limited  $\Delta H$  range on either side of the turning point where the feature occurs. For example,  $H_p$  is defined by the intersection of two linear fits to the data, one roughly in the range of  $H_{\text{on}}$  to  $H_p$  and one in the range of  $H_p$  to  $H_0$ . In Fig. 7a we show the positions of  $H_1$ ,  $H_{\text{knee}}$ ,  $H_p$ , and  $H_{c2}^{\text{av}}$  in  $H$  vs.  $T$  axes. In Fig. 7b we mark the positions of the onset, the peak, and the end of the peak effect, as well as the lower end ( $H_0$ ) and the midpoint ( $H_{c2}^{\text{av}}$ ) of the  $H_{c2}$  transition in  $\Delta H$  vs.  $H_{c2}^{\text{av}}$  axes. It is evident in the figure that the peak effect disappears when it crosses over into the  $H_0$  to  $H_{c2}^{\text{up}}$  range, where bulk superconductivity is partially lost due to sample inhomogeneity.

It is not clear whether the peak effect continues to exist with a reduced magnitude inside this region. It seems likely that its magnitude is reduced below detectable levels. This can be due to loss of superconductivity in regions of the sample and the resulting absence of bulk macroscopic critical current. However the peak effect continues to manifest itself in ac-susceptibility. This can be explained under the assumption that the screening supercurrent near the sample surface is assisted by the sheath of surface superconductivity. This picture also provides an explanation for the approximately simultaneous disappearance of the peak effect and surface superconductivity in previous studies.[8]

The observation with ac-susceptometry of a continuation of the peak effect line on the surface of the sample is an indication that the peak effect exists, though unobservable, at these lower fields, in isolated superconducting islands in the bulk of the sample as well. Moreover, as shown in Fig. 7, the linear extrapolation of the onset and the peak of the peak effect, as well as  $H_{c2}^{\text{av}}$ , merge at a field of approximately 850 Oe, suggesting that this may indeed be the vicinity of the critical point where the first-order phase transition underlying the peak effect ends.

## 7. The $H_{c2}$ and $T_{c2}$ transition lines

The nature of the MCP which was previously identified by Park *et al.*[8] remained unresolved. Our current findings suggest that surface superconductivity plays only a coincidental role in the disappearance of the peak effect. Thus, the nature of the MCP is determined

from the nature of the  $H_{c2}$  and  $T_{c2}$  lines discussed in section I.

We have a means of comparing the  $H_{c2}$  and  $T_{c2}$  transitions. The approximate location of the MCP in ac-susceptometry is at  $T = 8.1$  K,  $H = 900$  Oe. The disappearance of the peak effect below 1718 Oe in the magnetocaloric measurements but only below approximately 900 Oe in ac-susceptometry, allows us to compare the transitions into the bulk normal state on the two sides of the MCP. As shown in Fig. 6c, all the curves with  $H_{c2}^{\text{av}} < 1718$  Oe (or equivalently  $T > 7.18$  K) for both increasing and decreasing fields collapse strikingly on two different curves. These data include transitions on both sides of the MCP. This suggests that the phase transitions out of the Bragg Glass ( $H_{c2}$ ) and disordered ( $T_{c2}$ ) phases are of the same nature. In other words, well defined vortices exist in the disordered vortex state above the peak effect. Here “well defined” is taken to mean that their magnetocaloric signature is indistinguishable from the one obtained in the transition between the normal and the Bragg Glass phases. However, it has to be borne in mind that changes in critical behavior can be subtle and hard to identify in our sample which shows significant inhomogeneity broadening.

We can overcome this difficulty and look for changes in critical behavior by integrating the normalized experimental curves. This way, a change or a trend in critical behavior obscured by inhomogeneity broadening will be more easily discerned as a trend in the computed integrals. The computed integrals of the normalized increasing ( $\mathcal{F}_{\text{up}}$ ) and decreasing ( $\mathcal{F}_{\text{down}}$ )

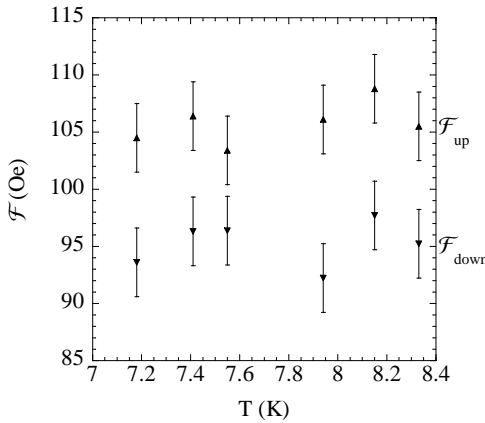


FIG. 8: Integrals of the rescaled ( $ds/dH$ ) for  $\Delta H$  from  $-150$  Oe to  $30$  Oe, for increasing ( $\mathcal{F}_{\text{up}}$ ,  $\blacktriangle$ ) and decreasing ( $\mathcal{F}_{\text{down}}$ ,  $\blacktriangledown$ ) fields. The peak effect feature was not observed at these temperatures. The error bars reflect the uncertainty in alignment of the magnetocaloric curves. Temperatures above  $8.15$  K correspond to the  $H_{c2}$  line of transitions proposed by Park *et al.*[8]

field curves around the region of the upper critical field are shown in Fig. 8. The integration has been performed between  $\Delta H = -150$  Oe and 30 Oe in the aligned axis. More explicitly:

$$\mathcal{F} = \int_{\Delta H = -150}^{\Delta H = 30} (ds/dH)_{normalized} d(\Delta H).$$

The error bars arise from the alignment uncertainty. All temperatures refer to the  $T_{c2}$  transition, except for the two marked with an asterisk which correspond to  $H_{c2}$ . We see no systematic trend in the result in any of the available temperatures. In conclusion, as far as the inhomogeneity of our sample allows us to discern, there is no detectable change between the low-field  $H_{c2}$  transition and the high-field  $T_{c2}$  transition to the normal state.

### 8. End of the peak effect

Finally, we discuss the “end” of the peak effect. Its position in the phase diagram is shown in Fig. 7b. In our data  $H_{\text{end}}$  occurs in a range between 32 and 39 Oe below  $H_{c2}^{\text{up}}$  and slightly above the position of the average superconducting transition,  $H_{c2}^{\text{av}}$ .  $H_{\text{end}}$  has been identified as the field at which a superconducting network which can support a macroscopic screening supercurrent forms inside the sample. The “end” feature occurs slightly above the midpoint of the  $H_0$  to  $H_{c2}^{\text{up}}$  range, as shown in Fig. 7b. This indicates that the critical current appears when roughly half of the sample is in the mixed state while the rest is still in the normal state. This observation is very interesting but requires further investigation. The role of surface superconductivity in establishing macroscopic supercurrents in the superconducting network can be examined experimentally.

## B. Discussion

### 1. Surface barrier, flux-flow heating, critical state screening

We can extend the conclusions from our measurements by evaluating the results of non-equilibrium and irreversible processes in the magnetocaloric effect.

We start with the surface barrier. Its presence results in delay of flux entry into the sample on increasing fields, up to a field approximately equal to the thermodynamic critical field,  $H_C$ .[21] In addition, the surface barrier has the more subtle consequence of introducing an asymmetry between the measured  $\Delta T$  on increasing and decreasing fields. On increasing

fields, vortices have to enter the sample through an energy barrier in a vortex free region.[22, 23] In this process, energy is dissipated approximately at a rate

$$\Phi_0 \cdot ((H_C^2 + H^2)^{1/2} - H) \cdot (V/4\pi) \cdot dH/dt,$$

where  $V$  is the sample volume and  $H_C$  the thermodynamic critical field.

In our measurements, for example at  $H \approx 3000$  Oe, this amounts to approximately  $2 \mu\text{W}$ , and will reduce the (negative)  $\Delta T$  observed on increasing fields by roughly  $1 \text{ mK}$ . On decreasing fields, the surface barrier has essentially no effect, and no irreversible heating is expected.[22] An asymmetry of this kind is shown schematically in Fig. 9a, and it is present in our data, for example in Fig. 5b. Moreover, this type of asymmetry disappears for lower values of the critical field, where surface superconductivity has disappeared,[8] for example in Fig. 5c.

Flux flow heating of the sample also leads to a similar asymmetry between the ascending and descending field branches. On increasing fields the negative  $\Delta T$  is reduced and on decreasing fields the positive  $\Delta T$  increased. An order of magnitude estimate of flux-flow heating can be obtained on the basis of the Bardeen-Stephen model.[24] For a cylindrical sample of radius  $R$ , length  $L$ , and for smooth field ramping at a rate  $dH/dt$ , one obtains  $P_{ff} \approx 10^7 (dH/dt)^2 \pi R^4 L / (8\rho_{ff})$ . This turns out to be negligible for the field ramp rates, approximately  $1 \text{ Oe/sec}$ , used in our measurements. We show the effect of this mechanism, grossly exaggerated, in Fig. 9b. Between the above two sources of irreversible heating, it is clear that low field ramp rates will render the latter ( $\propto (dH/dt)^2$ ) negligible, but will not reduce the effect of the former which scales as  $dH/dt$ , as does the magnetocaloric  $\Delta T$ .

Next we examine the case of a non-equilibrium critical state profile outside the peak effect region. A critical current that monotonically decreases with field, i.e. away from the peak effect region, will result in the opposite asymmetry than the one just mentioned. This is so, because on increasing fields the critical state profile becomes less steep, resulting in faster loss of flux than the field ramp rate, and thus increased  $\Delta T$ . The opposite occurs on decreasing fields, resulting in a lower  $\Delta T$  than indicated by the equilibrium  $T_s(\partial s/\partial H)_T$ . This mechanism is shown schematically in Fig. 9d. A simplified calculation for cylindrical sample geometry, like the ones found in the literature, [20, 25] yields an asymmetry factor in  $\Delta T$  equal to:

$$1 \pm (4\pi R/3c)(\partial J_c/\partial H)_T \quad (3)$$

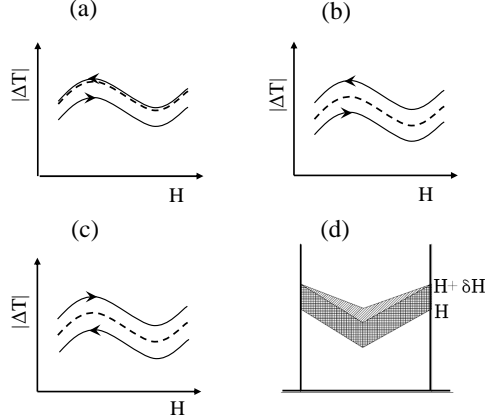


FIG. 9: (a)-(c) Schematic representations of the asymmetries induced by irreversible and non-equilibrium effects on the magnetocaloric measurement,  $|\Delta T|$ . The field ramp directions are indicated by arrows, and the equilibrium  $(\partial s / \partial H)_T$  curve corresponds to the dashed line. (a) Surface barrier heating. (b) Flux flow heating. (c) Critical state screening.

(d) Qualitative schematic of the evolution of the critical state field profile, for increasing field and  $\partial j_c / \partial H < 0$ . When the applied field increases from  $H$  to  $H + \delta H$ , the flux increase corresponds to the total shaded area, not just the lower shaded part. This results in increased magnetocaloric signal, as shown in (c) and discussed in the text.

for increasing (−) and decreasing (+) fields. Here,  $R$  is the sample radius and  $J_c(H)$  the  $H$  dependent critical current. Moreover it is assumed that the critical state field profile does not result in significant modification of the critical current in the sample interior. Nevertheless, even in the case where the value of the critical current varies spatially inside the sample,  $J_c = J_c(B(r))$ , the same type of asymmetry results, with slightly modified value though. The derivation of the above factor is outlined in the appendix. This asymmetry is illustrated in Fig. 9c. This type of asymmetry is only observed in our data in the region of the upper critical field and the peak effect.

For example, in data without peak effect, as shown in Fig. 5c, the magnetocaloric curves are reversible outside a region between  $H_{\text{hyst}}$  and  $H_{c2}^{\text{up}}$  but consistently show hysteresis in that region, see also Fig 6b. This behavior can be attributed to critical state screening. Then, the hysteresis which persists almost all the way up to  $H_{c2}^{\text{up}}$  indicates that the critical current is nonzero arbitrarily close to the upper critical field, and vanishes abruptly only at a distance of 10 -30 Oe from  $H_{c2}^{\text{up}}$ . In addition, the lack of asymmetry in the increasing and

decreasing field curves below the hysteretic region, implies that the critical current density varies very weakly with applied field. More specifically, the asymmetry in any of the data without peak effect is less than 5% of the magnitude of  $(ds/dH)$ . By Eq. 3 we obtain

$$(\partial J_c / \partial H)_T < (1/2) \cdot 0.05 \cdot (3c/4\pi R) \approx 0.36 \text{ A/cm}^2 \text{ Oe},$$

where the numerical result is expressed in conventional units for convenience.

## 2. Critical current estimates

From the measurements we can estimate the value of the critical current before it vanishes in the upper critical field region, in the context of critical state screening. We assume that the entropy per vortex is essentially constant in the neighborhood of the upper critical field and the peak effect.[29] Therefore changes in magnetic flux ( $\Delta\Phi$ ) are proportional to changes in entropy,  $\Delta\Phi \propto \Delta S$ . Then an integral of  $ds/dH$ , such as  $\mathcal{F}_{up}$  and  $\mathcal{F}_{down}$ , can be approximately taken to represent a change in magnetic flux in the sample. In the critical state model, we can relate changes in flux to the critical current.

At the temperatures where no peak effect is observed, we estimate the critical current in the neighborhood of  $H_{hyst}$ . For simplicity we consider a linear field profile in the sample, with slope

$$dH/dr = (4\pi/c) J_c,$$

where  $r$  is the radial distance from the axis of the (cylindrical) sample. In the vicinity of  $H_{hyst}$  simple integration gives a macroscopic magnetic flux difference ( $\Delta\Phi$ ) between the increasing and decreasing field branch approximately equal to:

$$\Delta\Phi = \left(1 + \frac{1}{\zeta}\right) (16\pi^2/3c) J_c(H_{hyst}) R^3.$$

see Eq. A.2 in the appendix. Due to the normalization performed for the integrals in Fig. 8 the flux difference is also approximately given by:

$$\Delta\Phi = (\mathcal{F}_{up} - \mathcal{F}_{down}) \pi R^2.$$

These two relations, allow us to obtain estimates for the critical current in the sample before this collapses to zero in the upper critical field region. We show these in Fig. 10, for temperatures above 7K, corresponding to the symbol for  $J_c$ . One should note that

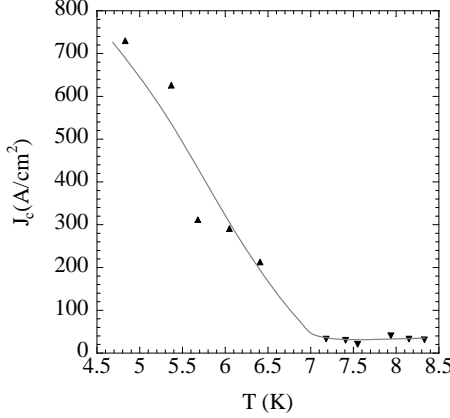


FIG. 10: Estimated values of critical current in the neighborhood of the upper critical field in our sample. For  $T > 7$  K we show  $J_c$  (marked by  $\blacktriangledown$ ), the critical current at the limit of hysteresis,  $H_{\text{hyst}}$ , in temperatures where no peak effect was observed. At temperatures below 7.18 K where peak effect was observed we show  $J_c^p$  ( $\blacktriangle$ ), the estimated critical current at the peak of the peak effect. The line is a guide to the eye.

critical currents with the values given for  $J_c$  in the figure, will lead to radial variation of the induction inside the sample by roughly 10 Oe. Due to the constraint imposed on  $(\partial J_c / \partial H)_T$ , (see discussion above), the critical current density will vary inside the sample due to screened induction by less than  $3.6 \text{ A/cm}^2$ . This represents only 10% of its value, and thus the assumption that the slope of the critical state profile (i.e.  $J_c(r)$ ) is essentially constant is self consistent.

A similar procedure can be followed for the curves showing the peak effect, in order to estimate the critical current at the peak of the peak effect. This is most easily done for the decreasing field, curves, under the additional assumption that the critical current increases linearly from zero at  $H_{\text{end}}$  to  $J_c^p$  at  $H_p$ . The integration relating the screened flux ( $\Delta\Phi$ ) to these three quantities leads to the rather complicated equation:

$$\left\{ \Delta H - \frac{\Delta\Phi}{\pi R^2 (1 + \frac{1}{\zeta})} \right\} x^2 - 2\Delta H x + 2\Delta H = 2\Delta H e^{-x}, \quad (4)$$

where  $\Delta H = H_{\text{end}} - H_p$ ,  $x = (4\pi R J_c^p) / (c \Delta H)$ . The screened flux for a curve with peak effect is obtained via integration between  $H_p$  and  $H_{c2}^{\text{up}}$  with respect to the universal curve of Fig. 6b (bottom). The resulting equations are solved numerically, and the results for  $J_c^p$  are shown in Fig. 10. The value at 6.79 K is not included, because the peak effect is barely observable at that temperature, which makes the procedure we outlined inapplicable.

### 3. Low field hysteresis: alternative interpretaion

We return to the low-field hysteresis near  $H_{c2}$ , illustrated in Fig. 5b. The combination of hysteretic and reversible behavior in the vicinity of  $H_{c2}$  is striking. Furthermore this behavior persists in all of the measurements which do not show the peak effect, down to an upper critical field of 676 Oe. In addition, we suggested earlier that the disappearance of the peak effect in our bulk measurements is due to loss of superconductivity in parts of the sample, while in ac-susceptometry it is due to the disappearance of surface superconductivity. Thus the possibility arises that the peak effect continues to exist at low fields, but it is not observable with the techniques used so far. In other words, our data raise the question whether the hysteretic order-disorder transition reported previously[5] continues down to low fields, where no peak effect is observed, but hysteresis occurs over a range too narrow to be detectable in neutron scattering. In this scenario, the hysteresis seen in Fig. 5c is related to a first order phase transition. If this is the case the hysteresis presented here will be observable in high resolution calorimetric measurements.

### 4. The “knee” feature

Finally we return to the newly identified “knee” feature, shown in Fig. 4c. From the occurrence of the knee in both ramp directions we conclude that it corresponds to an equilibrium feature of the thermodynamic behavior inside the Bragg Glass phase. To appreciate this argument, note that all three sources of irreversible and non-equilibrium effects discussed at the beginning of this subsection, will induce asymmetry on the  $(ds/dH)$  curves for opposite field-ramp directions. For example, the two curves of Fig. 4c show asymmetry, as already mentioned. This is due to surface barrier-related heating on increasing field. On the other hand, symmetric trends in the measured  $(ds/dH)$  curves have to be related to equilibrium behavior, and we thus conclude that  $H_{\text{knee}}$  corresponds to an equilibrium feature. Neutron scattering did not reveal any structural changes in the vortex lattice[5, 8] around  $H_{\text{knee}}$ , which suggests that the nature of this feature is rather subtle. It would be interesting to investigate the corresponding part of the phase diagram for changes in dynamical response, as well as for a possible relation of this novel feature to the thermomagnetic instability in Nb.

### C. Summary

From the reported magnetocaloric-effect results, we gain a significant amount of novel information about the Nb sample previously studied using SANS and ac-susceptometry.

The upper critical field shows significant inhomogeneity broadening. The broad  $H_{c2}$  transition is related to the disappearance of the peak effect in bulk measurements. The peak effect disappears in the phase diagram when it enters the range where regions of the sample are normal. Yet, magnetic irreversibility, indicating nonzero critical currents, occurs when regions of the sample are normal. The peak effect is observable with ac-susceptometry at fields much lower than with magnetocaloric measurements. In the former case screening occurs locally, near the surface,[8] presumably assisted by a superconducting surface layer. This could indicate that the peak effect still occurs in the bulk of the sample in regions that are superconducting.

The low field transition from the Bragg Glass phase into the normal state seems to be the same as the high field transition between the structurally disordered[5] vortex state and the normal state. Moreover, hysteresis occurs in magnetocaloric curves that do not display the peak effect, but in the neighborhood of this hysteresis the non-equilibrium and irreversible effect signatures that we discussed are absent. Finally a new feature corresponding to a knee in the magnetocaloric coefficient has been identified and its position mapped out in the phase diagram, Fig. 7 a. These new findings allow us to refine the previously proposed peak effect phase diagram (Fig. 1), but also point to an alternative picture.

In the multicritical point picture, the magnetocaloric-effect results reported here have strong implications for understanding the nature of the multicritical point where the peak effect disappears.[8, 9, 10] A tricritical point can be ruled out since the change in slope between the  $H_p$  and low field  $H_{c2}$  lines would lead to violation of the  $180^\circ$  rule[8, 30] imposed by thermodynamics. The fact that the magnetocaloric transition appears to be continuous and of the same character across both  $T_{c2}$  and  $H_{c2}$ , suggests that the critical point is bicritical. Bicriticality implies the competition of two bulk vortex phases, an ordered Bragg glass[2, 3] and a disordered vortex glass. The vortex glass phase is not necessarily superconducting in the sense of the original proposal,[31] but it has to be a genuine phase possessing an order parameter absent in the normal state,[33] and *in competition* with that of the Bragg glass. In addition, it possesses superconducting phase rigidity even under partial loss of bulk

(mixed state) superconductivity.

Finally, we wish to discuss an alternative picture in which the order-disorder transition does not end at the previously identified critical point. The experimental disappearance of the peak effect in magnetocaloric measurements may be due to sample inhomogeneity. In addition, the peak effect disappears in ac-susceptometry due to the disappearance of surface superconductivity.[8] Nevertheless, the vortex lattice disordering transition can continue to lower fields, where the peak effect is not detectable. Hysteresis related to a first order phase transition occurs over a narrow range in this part of the phase diagram, and the width of the hysteresis region grows appreciably only at higher fields where the peak effect is sufficiently far from the  $H_{c2}$  region. In this picture, no critical point associated with the disordering transition exists at any finite field or temperature.[33]

#### IV. CONCLUSIONS

We have identified the magnetocaloric signatures of the peak effect in a Nb single crystal. In addition we classified and outlined the various sources of irreversible and non-equilibrium effects occurring in such measurements and offered ways for their evaluation. With these in mind, magnetocaloric measurements prove very useful in studies of the mixed state. They are suitable for studying the upper critical field region. They allow the identification and study of dynamical effects, such as the onset, the peak and the end of the peak effect, and provide estimates of the critical currents involved. Moreover they are useful in identification of changes in thermodynamic behavior deeper inside the mixed state, e.g. the “knee” feature identified here.

With the wealth of novel information obtained in our measurements we were able to shed light into the disappearance of the peak effect in Nb. We refined the multicritical point scenario drawn previously.[8] In addition, based on experimental facts, we proposed an alternative scenario which can be experimentally tested.

We thank J. J. Rush and J. W. Lynn from NIST for providing the Nb crystal and acknowledge numerous helpful discussions with D. A. Huse, J. M. Kosterlitz and M. C. Marchetti. This work was supported by NSF under grant No. nsf-dmr 0406626.

## APPENDIX: MAGNETIC FLUX CHANGES DUE TO THE CRITICAL STATE

### 1. Asymmetry factor of $(ds/dH)$

First we derive the critical state asymmetry factor of  $(ds/dH)$  discussed in Section III B. We limit our discussion to cylindrical sample geometry, with the field applied along the cylindrical axis. The critical current is taken to depend on  $B$ , or equivalently on  $H$ . We focus on the region close to  $H_{c2}$ , where these are linearly related by :  $B = (1+1/\zeta)H - H_{c2}/\zeta$ , with  $\zeta = \beta_A (2\kappa^2 - 1)$ .[26] Due to critical current screening, the local induction (or field) inside the sample is modified with respect to the applied field and depends on radial distance from the axis ( $r$ ) of the sample:  $H = H(r)$ . From the Ampère law the field variation resulting from the critical current is:

$$\frac{dH}{dr} = \pm \frac{4\pi}{c} J_c(H(r)) ,$$

for increasing (+) and decreasing (−) field. The critical current depends on  $B$ , but we make the simplifying assumption that for a given value of applied field  $H_a$ , the local induction inside the sample leads to a negligible critical current variation:  $J_c(r) = J_c = \text{const.}$  In addition we neglect demagnetizing effects. We then obtain:

$$H(r) = H_a \pm (4\pi/c) J_c \cdot (r - R) ,$$

where  $R$  is the sample radius and again the solutions correspond to increasing (+) and decreasing (−) field. The corresponding magnetic induction is simply:

$$B(r) = \left\{ H_a \pm \frac{4\pi}{c} J_c \cdot (r - R) \right\} \cdot (1 + 1/\zeta) - H_{c2}/\zeta .$$

This is easily integrated over the cross sectional area of the sample, in order to obtain the magnetic flux through the sample:

$$\Phi = \int_0^R B(r) 2\pi r \cdot dr , \quad (\text{A.1})$$

to yield:

$$\Phi = \left\{ H_a \left( 1 + \frac{1}{\zeta} \right) - H_{c2}/\zeta \mp \left( 1 + \frac{1}{\zeta} \right) \frac{4\pi R J_c}{3c} \right\} \cdot \pi R^2 . \quad (\text{A.2})$$

Note that here the significance of the signs is reversed for increasing (−) and decreasing (+) field. The rate of change in magnetic flux through the sample for changes in applied field is:

$$\frac{d\Phi}{dH_a} = \left\{ 1 \mp \frac{4\pi R}{3c} \left( \frac{\partial J_c}{\partial H} \right)_T \right\} \cdot \left( 1 + \frac{1}{\zeta} \right) \cdot \pi R^2.$$

This is proportional to the magnetocaloric signal, and includes the asymmetry factor given in Eq. 3, with negative (−) sign for increasing field, positive (+) for decreasing.

## 2. Flux screening in the peak effect region

The critical current between  $H_p$  and  $H_{\text{end}}$  is taken to be:

$$J_c = \begin{cases} 0, & \text{if } H > H_{\text{end}} \\ J_c^p \left( \frac{H_{\text{end}} - H}{H_{\text{end}} - H_p} \right), & \text{if } H_p < H < H_{\text{end}} \end{cases}$$

Then the Ampère law for the field ( $H_p < H < H_{\text{end}}$ ) inside the sample is:

$$\frac{dH}{dr} = -\frac{4\pi J_c^p}{c} \cdot \left( \frac{H_{\text{end}} - H}{H_{\text{end}} - H_p} \right)$$

This is solved for applied field  $H_a = H_p$ , with the boundary condition  $H(r = R) = H_p$  (again by neglecting demagnetizing effects), and yields:

$$H(r) = H_{\text{end}} - (H_{\text{end}} - H_p) e^{(r-R)/l},$$

with  $l^{-1} = (4\pi J_c^p)/(c(H_{\text{end}} - H_p))$ . From this, the local induction is obtained, and via integration over the sample cross-section, see Eq. A.1 the magnetic flux through the sample is:

$$\begin{aligned} \Phi = & \left( 1 + \frac{1}{\zeta} \right) \\ & \times \left\{ H_{\text{end}} \pi R^2 - 2\Delta H \pi (Rl - l^2) - 2\Delta H \pi l^2 e^{-R/l} \right\} \\ & - H_{c2} \pi R^2 / \zeta, \end{aligned}$$

where we used the notation  $\Delta H = H_{\text{end}} - H_p$ . The flux in the absence of screening ( $J_c = 0$ ) is:

$$\Phi' = \left( 1 + \frac{1}{\zeta} \right) H_p \pi R^2 - H_{c2} \pi R^2 / \zeta.$$

Therefore the amount of screened flux  $\Delta\Phi = \Phi - \Phi'$ , turns out to be:

$$\begin{aligned}\Delta\Phi = & \pi R^2 \left( 1 + \frac{1}{\zeta} \right) \\ & \times \left\{ \Delta H - 2 \Delta H \left( \frac{l}{R} - \frac{l^2}{R^2} \right) - 2 \Delta H \frac{l^2}{R^2} e^{-R/l} \right\}.\end{aligned}$$

The additional definition  $x = R/l$ , straightforwardly leads to Eq.4:

$$\left\{ \Delta H - \frac{\Delta\Phi}{\pi R^2 \left( 1 + \frac{1}{\zeta} \right)} \right\} x^2 - 2\Delta H x + 2\Delta H = 2\Delta H e^{-x}.$$

---

[1] A. I. Larkin, Sov. Phys. JETP **31**, 784 (1970); Y. Imry and S. Ma, Phys. Rev. Lett. **35** 1399 (1975).

[2] T. Nattermann, Phys. Rev. Lett., **64**, 2454 (1990).

[3] T. Giamarchi and P. Le Doussal, Phys. Rev. Lett., **72**, 1530, (1994).

[4] D. Christen, F. Tasset, S. Spooner, and H. A. Mook, Phys. Rev. B **15**, 4506 (1977).

[5] X. S. Ling, S. R. Park, B. A. McClain, S. M. Choi,, D. C. Dender and J. W. Lynn , Phys. Rev. Lett. **86**, 712 (2001).

[6] A. M. Troyanovski, M. van Hecke, N. Saha, J. Aarts, and P. H. Kes, Phys. Rev. Lett. **89**, 147006 (2002).

[7] W. DeSorbo, Rev. Mod. Phys. **36**, 90 (1964).

[8] S. R. Park, S. M. Choi, D. C. Dender, J. W. Lynn, and X. S. Ling, , Phys. Rev. Lett. **91**, 167003 (2003)

[9] M. G. Adesso, D. Uglietti, R. Flukiger, M. Polichetti, and S. Pace, Phys. Rev. B **73**, 092513 (2006).

[10] D. Jaiswal-Nagar, D. Pal, M. R. Eskildsen, P. C. Canfield, H. Takeya, S. Ramakrishnan, and A. K. Grover, PRAMANA-J. of Phys. **66**, 113 (2006).

- [11] R. L. Cormia, J. D. Mackenzie, J. D. Turnbull, J. Phys. Chem., **65**, 2239 (1963); J. Dages, H. Gleiter, J. H. Perepezko, Mat. Res. Soc., *Symposium Proceedings*, **57** (1986); R. W. Cahn, Nature, **323**, 667 (1986).
- [12] R. Lortz, F. Lin, N. Musolino, Y. Wang, A. Junod, B. Rosenstein, and N. Toyota, Phys. Rev. B, **74** 104502 (2006).
- [13] N. Daniilidis *et al.* (*unpublished*).
- [14] Y. Shapira and L.J. Neuringer, Phys. Rev. **154**, 375 (1967).
- [15] I. K. Dimitrov, *Ph.D. Thesis*, Brown University (2007).
- [16] A. T. Fiory and B. Serin, Phys. Rev. Letters **16**, 308 (1966); F. A. Otter Jr., and P. R. Solomon, Phys. Rev. Letters **16**, 681 (1966).
- [17] In perfectly adiabatic conditions, the heat is “exchanged” within the superconductor itself resulting in a change of its temperature.
- [18] C. P. Bean and J. D. Livingston, Phys. Rev. Lett. **12**, 14 (1964).
- [19] J. Bardeen and M. J. Stephen, Phys. Rev. **140**, A1197 (1965).
- [20] C. P. Bean, Phys. Rev. Lett. **8**, 250 (1962).
- [21] P. G. deGennes, Solid State Commun. **3**, 127 (1965).
- [22] J. R. Clem, *Low Temperature Physics-LT13*, edited by K. D. Timmerhaus, W. J. O’Sullivan, and E. F. Hammel (Plenum, New York, 1974), Vol. 3, p.102.
- [23] L. Burlachkov, Phys Rev. B **47**, 8056 (1993).
- [24] J. Bardeen and M. J. Stephen, Phys. Rev. **140**, A1197 (1965).
- [25] Ming Xu, Phys. Rev. B, **44**, 2713 (1991).
- [26] P. G. deGennes, *Superconductivity of metals and alloys*, W. A. Benjamin Inc., New York, Amsterdam, 1966.
- [27] S. P. Farrant and C. E. Gough, Phys. Rev. Lett. **34**, 943 (1975).
- [28] D. J. Thouless, Phys. Rev. Lett. **34**, 947 (1975)
- [29] A possible change of vortex entropy at the peak effect is expected to be very small, if present, and is certainly not detectable with our technique.
- [30] J. C. Wheeler, Phys. Rev. A **12**, 267 (1975).
- [31] D. S. Fisher, M. P. A. Fisher, and D. A. Huse, Phys. Rev. B **43**, 130 (1991).
- [32] T. Nattermann and S. Scheidl, Adv. Phys **49**, 607 (2000).
- [33] G. Menon Phys. Rev. B **65**, 104527 (2002).